Supplementary Information

Title: An aptamer-based magnetic flow cytometer using matched filtering

Author names and affiliation: Chih-Cheng Huang[a], Partha Ray[b], Matthew Chan[c], Xiahan Zhou[c], and Drew A. Hall[c,d]

[a] Materials Science and Engineering Program, University of California – San Diego, La Jolla, CA 92093, USA

[b] Division of Surgical Oncology, Department of Surgery, Moores Cancer Center, UC San Diego Health, La Jolla, CA 92093, USA

[c] Department of Electrical and Computer Engineering, University of California – San Diego, La Jolla, CA 92093, USA

[d] Department of Bioengineering, University of California – San Diego, La Jolla, CA 92093, USA

Corresponding author: drewhall@ucsd.edu

Abstract: Facing unprecedented population-ageing, the management of noncommunicable diseases (NCDs) urgently needs a point-of-care (PoC) testing infrastructure. Magnetic flow cytometers are one such solution for rapid cancer cellular detection in a PoC setting. In this work, we report a giant magnetoresistive spin-valve (GMR SV) biosensor array with a multi-stripe sensor geometry and matched filtering to improve detection accuracy without compromising throughput. The carefully designed sensor geometry generates a characteristic signature when cells labeled with magnetic nanoparticles (MNPs) pass by thus enabling multi-parametric measurement like optical flow cytometers (FCMs). Enumeration and multi-parametric information were successfully measured across two decades of throughput (37 – 2730 cells/min). 10-μm polymer microspheres were used as a biomimetic model where MNPs and MNP-decorated polymer conjugates were flown over the GMR SV sensor array and detected with a signal-to-noise ratio (SNR) as low as 2.5 dB due to the processing gain afforded by the matched filtering. The performance was compared against optical observation, exhibiting a 92% detection efficiency. The system achieved a 95% counting accuracy for biomimetic models and 98% for aptamer-based pancreatic cancer cell detection. This system demonstrates the ability to perform reliable flow cytometry toward PoC diagnostics to benefit NCD control plans.

Keywords: Aptasensor, Flow Cytometry, Magnetic Biosensor, Matched Filter, Pancreatic Cancer, Point-of-Care (PoC) testing

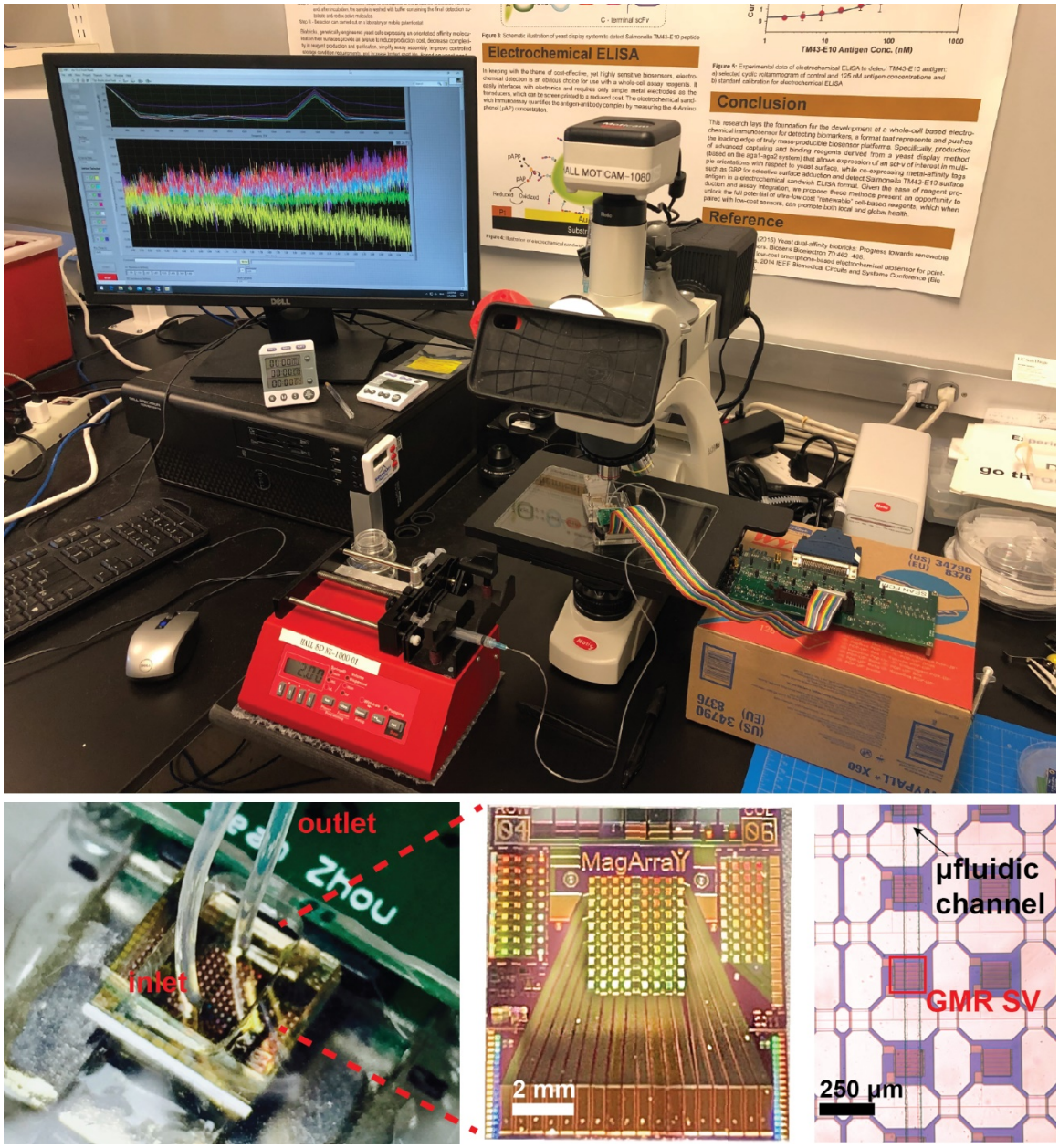

Supplemental Figure 1. Photographs of the system (top) and zoomed-in view (from bottom left to right) of the sensor setup, a sensor chip, and the microfluidic channel. The desktop-based testing setup shows the MFC system and all components. Measurements were recorded through a custom written LabVIEW interface (as shown on PC screen).

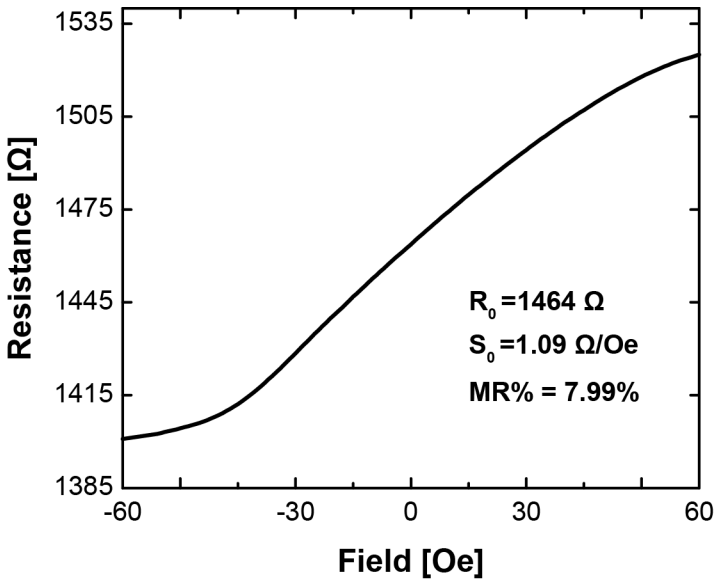

Supplemental Figure 2. Measured magnetoresistance (MR) curve of GMR SV sensor. Each GMR SV has a nominal resistance (R_0) of 1464 Ω, magnetoresistance (MR) ratio of 7.99%, and a sensitivity of 1.09 Ω/Oe.

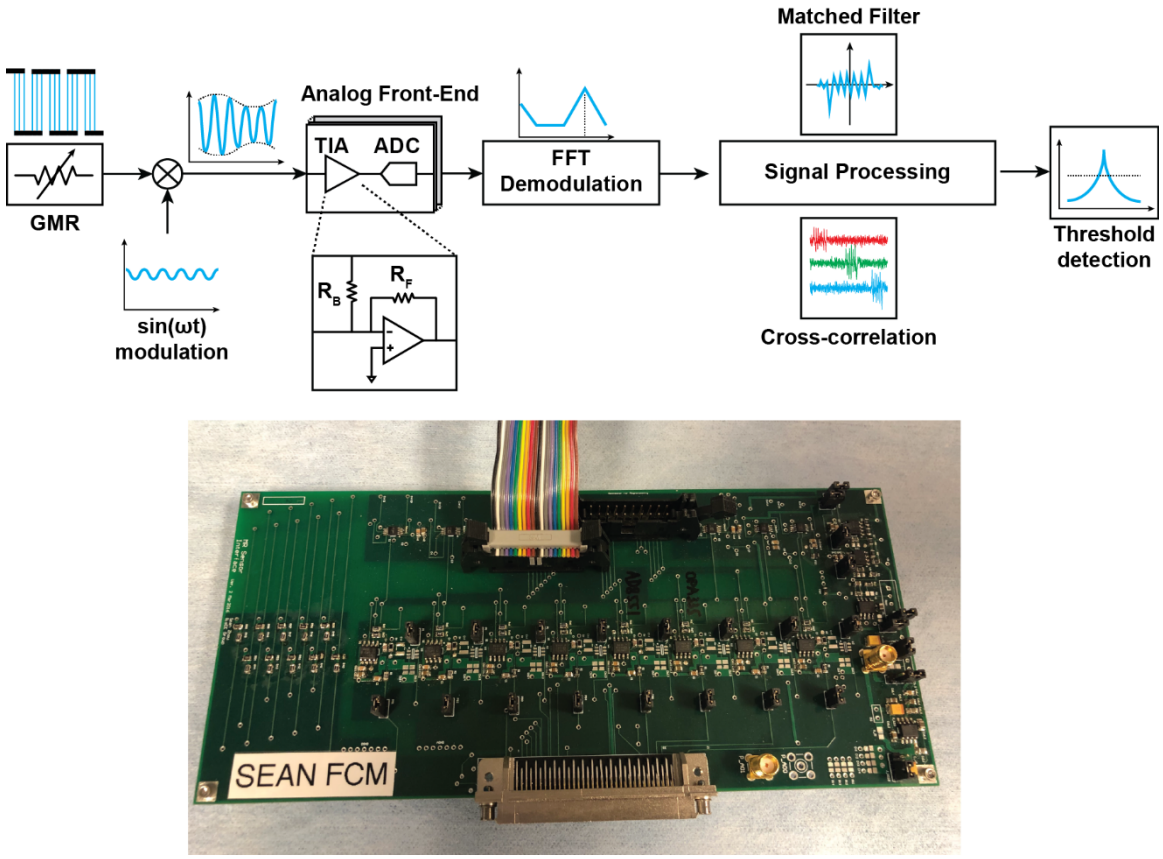

Supplemental Figure 3. Block diagram of the measurement electronics and photograph of the PCB. The GMR sensors are modulated by a sinusoidal voltage and the resulting currents are quantized by a transimpedance amplifier (TIA) and an ADC. A bleed resistor (R_B) removes most of the sensor baseline current. Digital signal processing performs demodulation then applies matched filtering and cross correlation to enable high SNR signal detection.

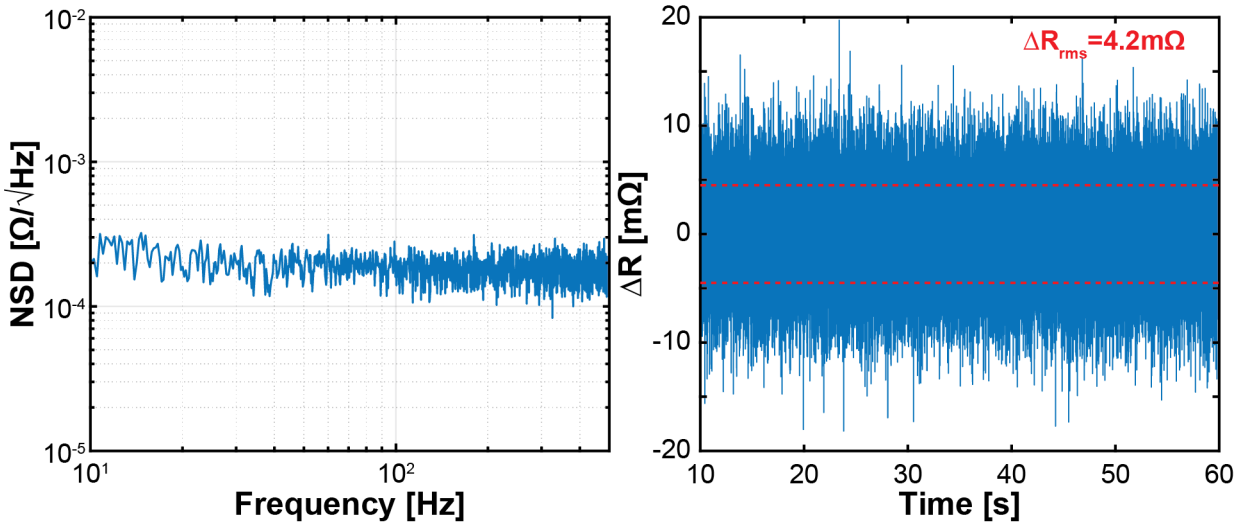

Supplemental Figure 4. Measured spectrum and noise (left). The noise is white over the bandwidth. Measured transient noise (right).

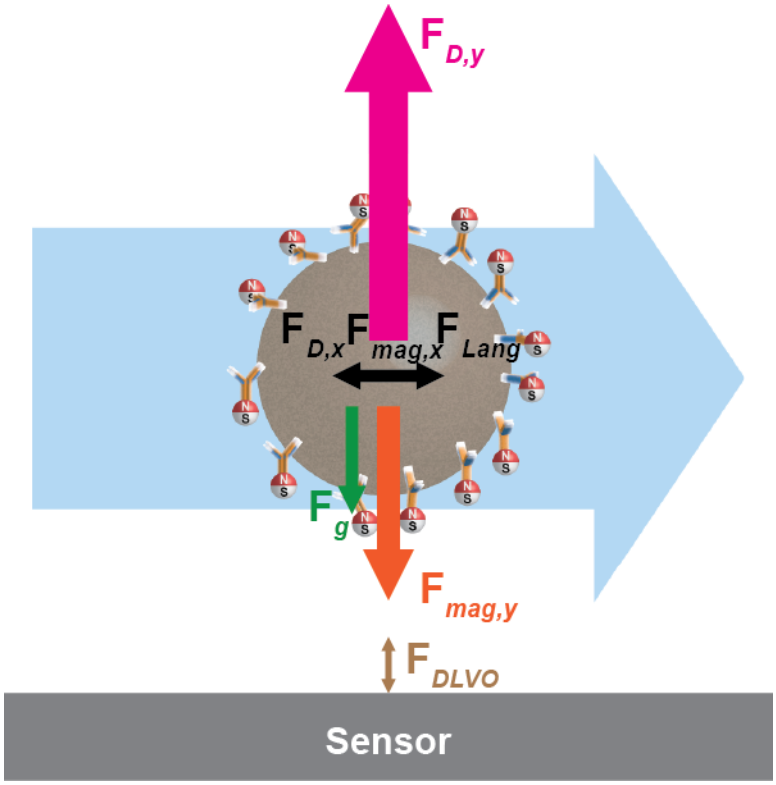

Supplemental Figure 5. Illustration of forces acting on a magnetic nanoparticle labelled analyte. Pumping rate and corresponding flow velocity fast enough to keep drag force dominant over other forces.

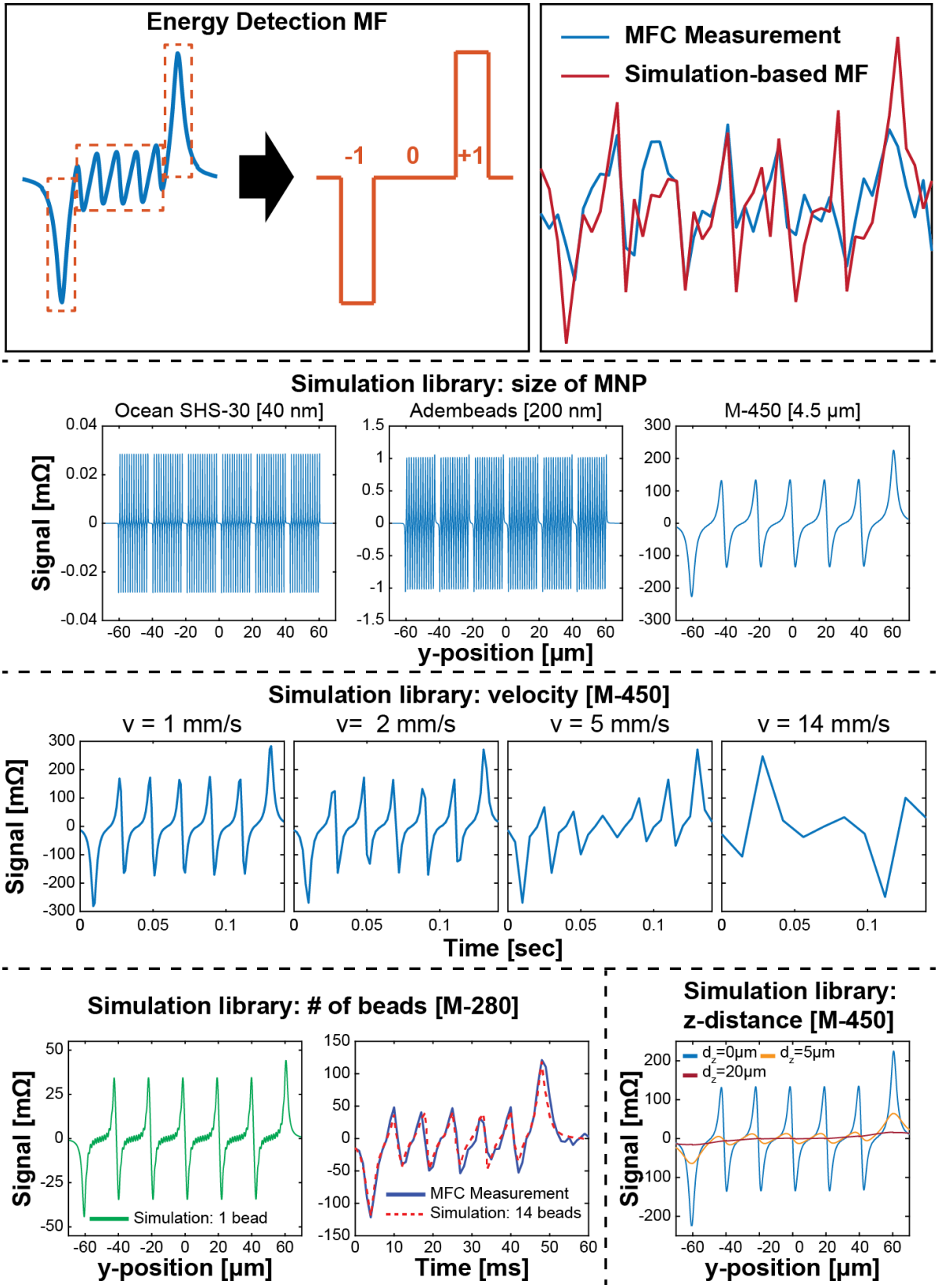

Supplemental Figure 6. EDMF and SMF templates. EDMF digitalizes signatures into three regions: -1, 0, and 1. SMF are based on MATLAB simulations with different parameters: MNP size, flow height (distance from sensor surface), number of MNPs, and velocity.

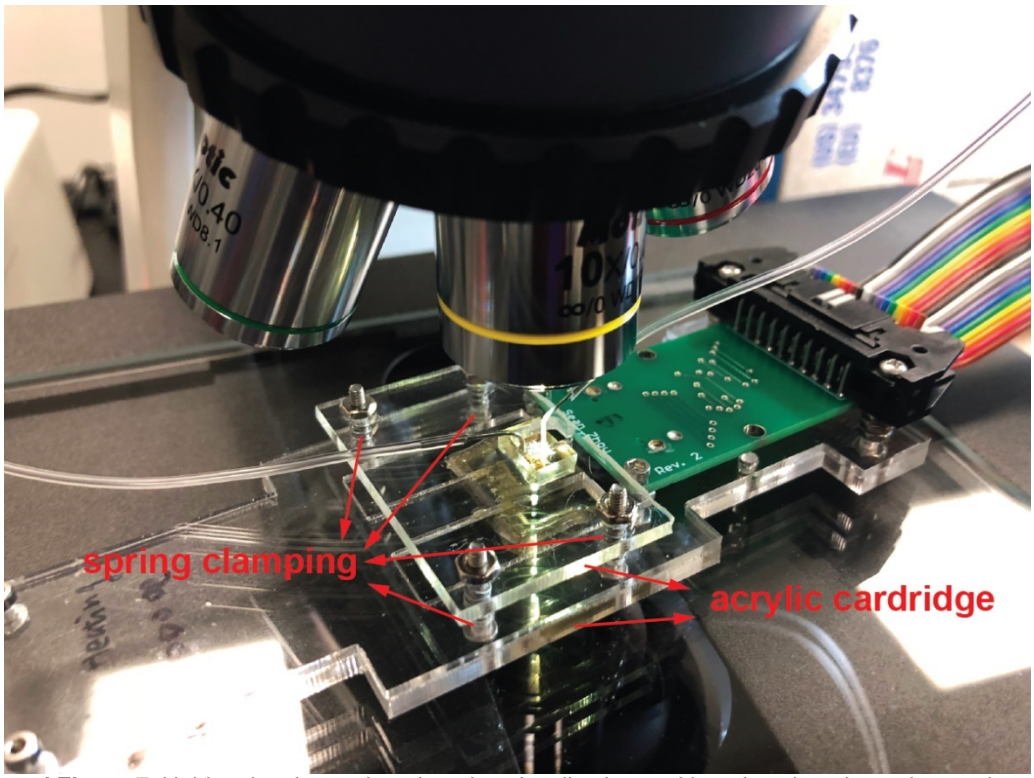

Supplemental Figure 7. Holder showing spring-clamping. Acrylic plates with spring clamping enhance the sealing and prevent the system from leaking.

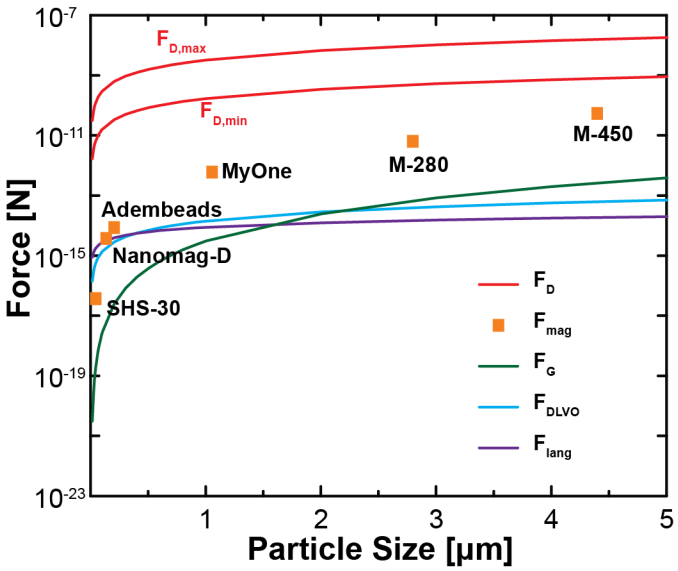

Supplemental Figure 8. Hydrodynamic analysis. For sub-micron-sized MNPs (Adembeads, 200nm; Nanomag-D, 130nm; and SHS-30, 40nm), the magnetic force is comparable to DLVO forces and Langevin force. While Drag force was kept dominant over other forces in the setup to allow samples flowing at middle of the channel and thus extract the multi-parametric information, as shown in the figure, drag force is at least one decade larger than magnetic force even flowing the largest MNP (M-450, 4.5 μm).

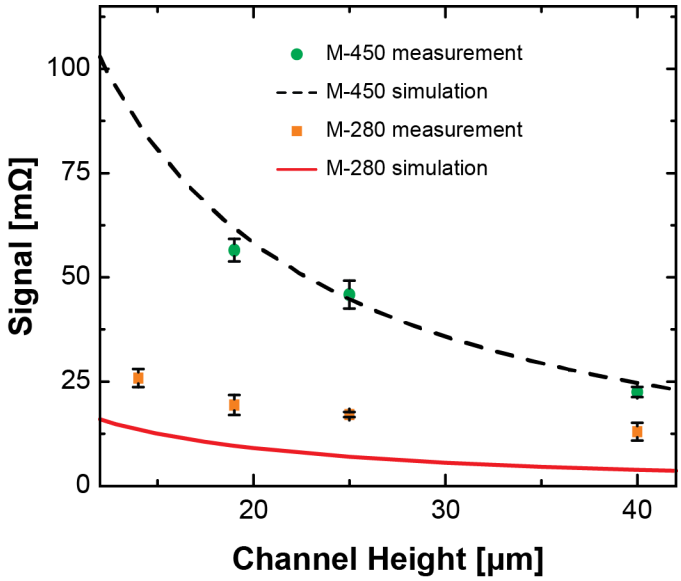

Supplemental Figure 9. Comparison of measured results and simulations using Dynabeads (M-450 and M-280). The experimental result of M-450 is in excellent agreement with the simulation, while the average signal amplitude of M-280 deviated from the theoretical prediction owing to the aggregation and/or chaining.

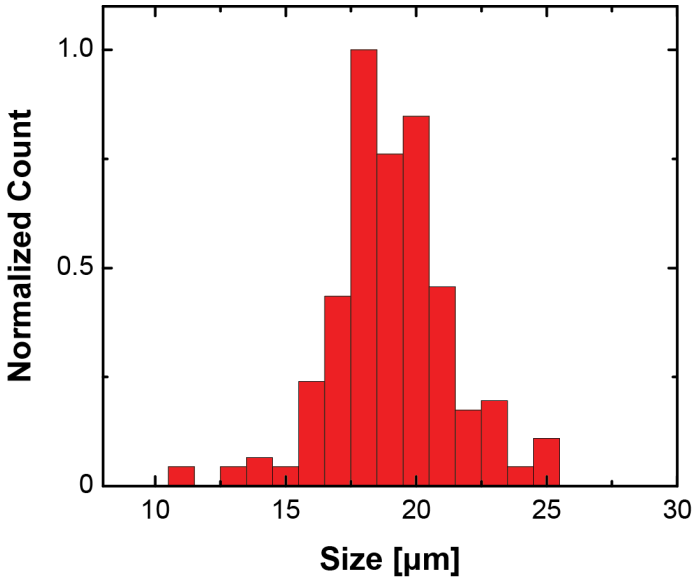

Supplemental Figure 10. Size distribution of Panc-1 cancer cells. The cell size of Panc-1 cells was calculated using a Vi-CELL XR Cell Viability Analyzer (Beckman Coulter). The mean cell diameter size was calculated to be 19.51 μm.

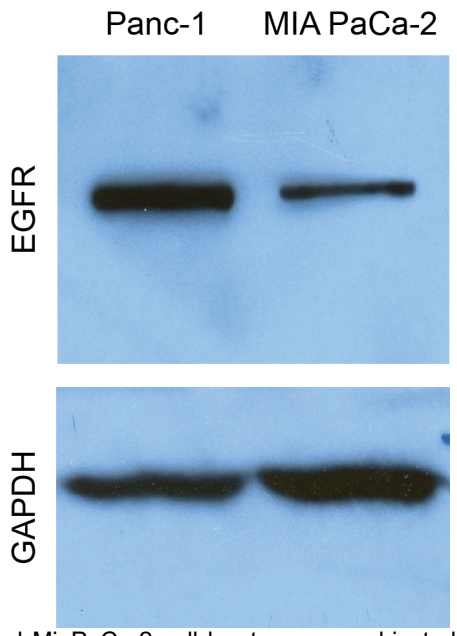

Supplemental Figure 11. Panc-1 and MiaPaCa-2 cell lysates were subjected to Western blot analysis using anti-EGFR antibody. Glyceraldehyde 3-phosphate dehydrogenase (GAPDH), a house keeping protein, was used as the loading control. Panc-1 cells expressed more EGFR as compared to the MiaPaca-2 cells.

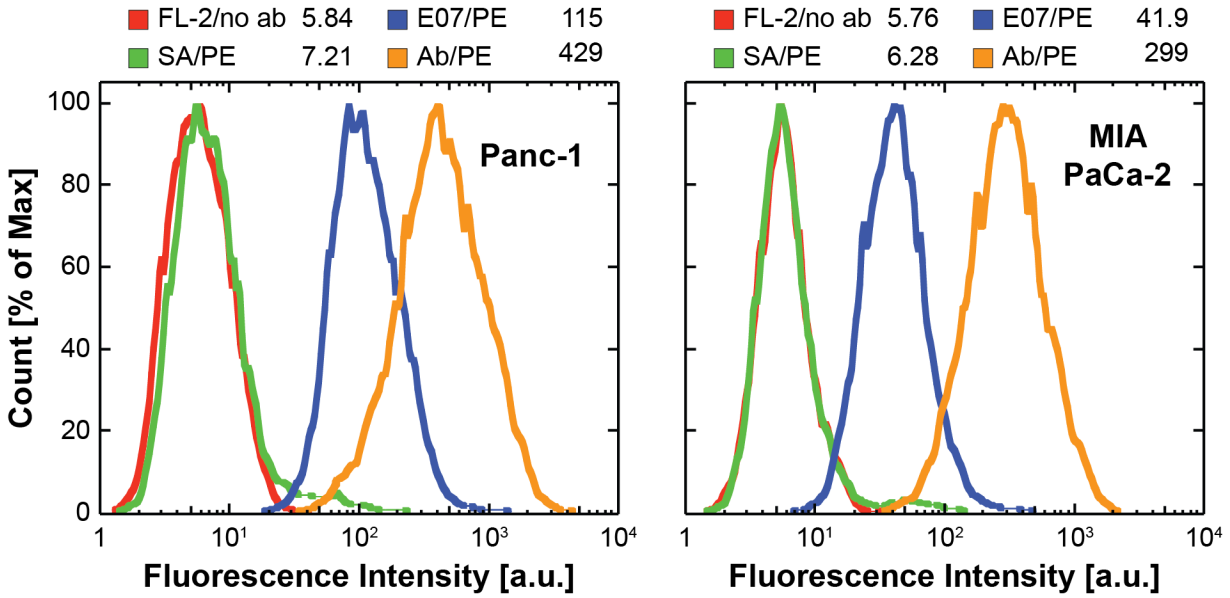

Supplemental Figure 12. Optical FCM data for Panc-1 and MiaPaCa-2 with E07 aptamer and anti-EGFR antibody. Optical FCM analyses of anti-EGFR aptamer (E07) and antibody binding to the Panc-1 and MiaPaCa-2 cells were performed by treating the cells with the fluorophore phycoerythrin (PE)-conjugated 5´Biotin-E07 aptamer (blue) or PE-conjugated Biotin-anti-EGFR antibody (orange). Streptavidin-PE was used as the negative binding control (green). The data was analyzed, and the mean fluorescence intensity (MFI) was calculated from the histogram plots.

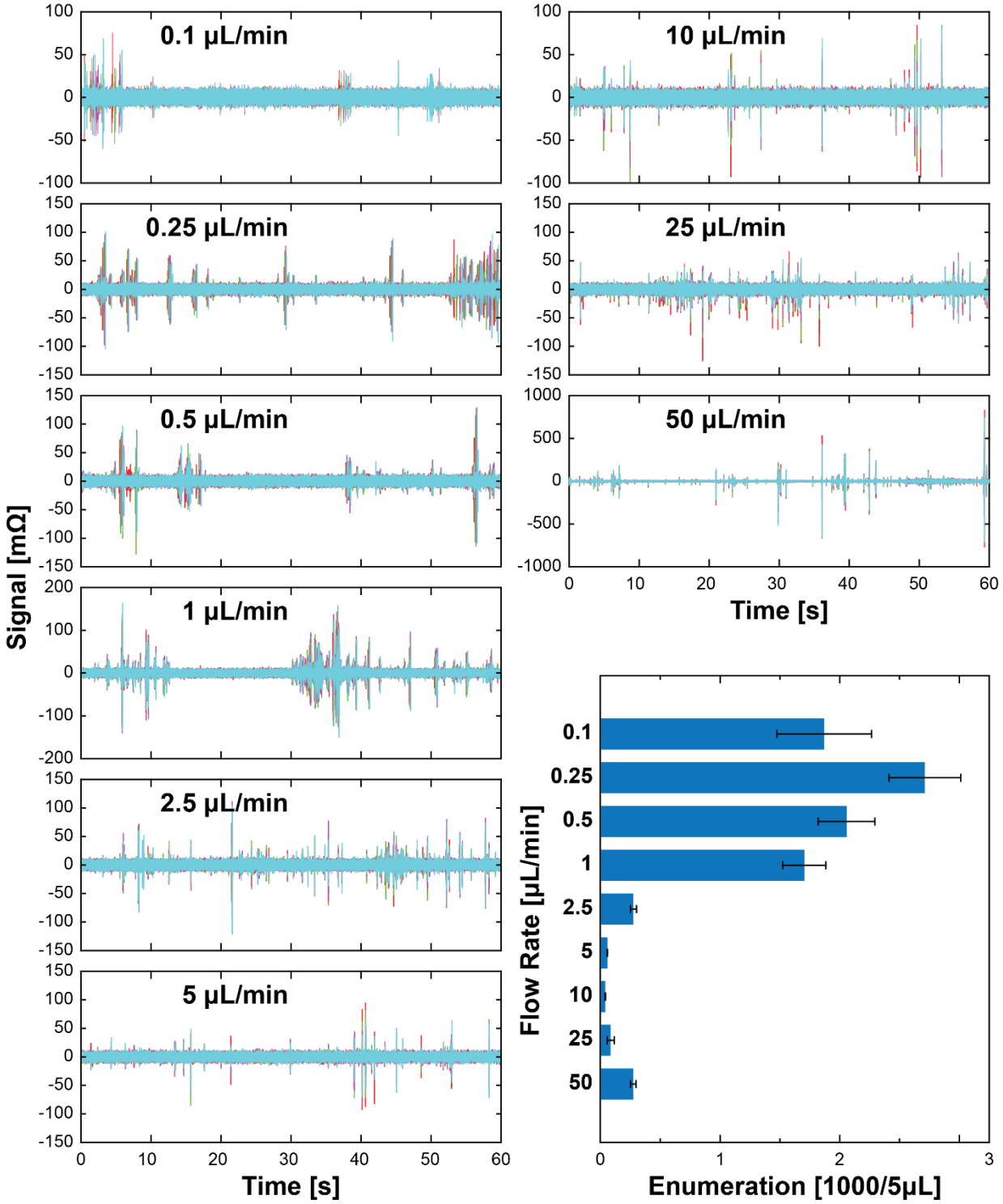

Supplemental Figure 13. MFC measurements through varying throughputs across four sensors. The E07-decorated Panc-1 cells were measured in culture media using the same procedure. The data shows successful enumeration across two decades of throughput, ranging from 0.1 to 50 µL/min. Due to the viscosity (Momen-Heravi et al., 2012), the enumeration (n = 2711) and the best throughput (0.25 µL/min) for measurements were different from what was measured in **Fig. 5B** (n = 7140 under 0.1 µL/min). The distorted signal and sample aggregation occurred more frequently when throughput was increased, while Panc-1 cells were still also measurable (n = 273) under 50 µL/min of throughput.

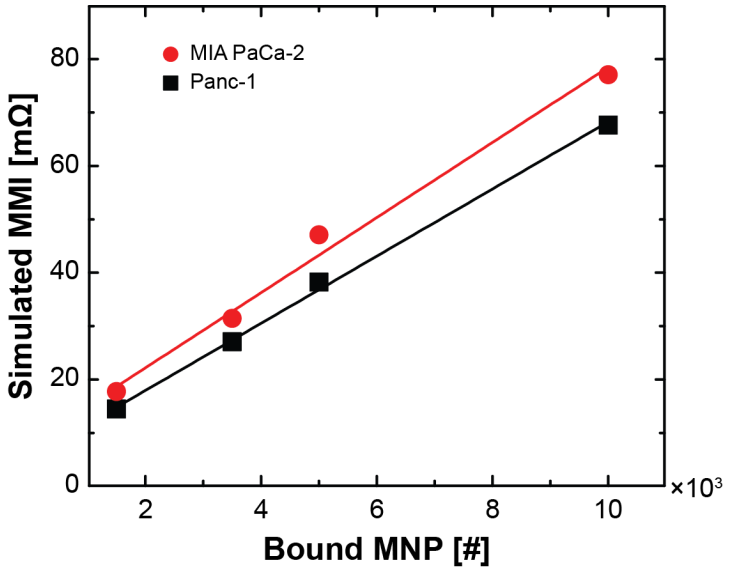

Supplemental Figure 14. Simulated magnetic signal vs. number of bound MNPs to both Panc-1 and MiaPaCa-2 cells. In the simulation, the cell was regarded as a sphere with random distribution of surface EGFR, and each EGFR can be bound with one MNP. Due to the smaller size of MiaPaCa-2 (mean diameter = 16.71 μm) and proximity sensing of magnetism, its signal would be larger than Panc-1 if they have the same amount of bound MNPs.